Geophysical Research Letters

RESEARCH LETTER
10.1029/2025GL120669

Deep Learning Identifies the Climate Warming Signal in Global Ocean Chlorophyll From Satellite Records

Lei Lin[1,2], **Chen Dong**[1], **Stephanie Henson**[3], **and Bingzhang Chen**[2]

[1]College of Ocean Science and Engineering, Shandong University of Science and Technology, Qingdao, China, [2]Department of Mathematics and Statistics, University of Strathclyde, Glasgow, UK, [3]National Oceanography Centre, Southampton, UK

Key Points:

- A deep learning model was developed and successfully detected the climate warming signal in global satellite chlorophyll-a data
- Deep learning indicates a fundamental difference in the chlorophyll-a response to climate warming compared to natural variability
- Global chlorophyll-a trends, especially in eastern and western boundary regions, were most sensitive to warming

Supporting Information:

Supporting Information may be found in the online version of this article.

Correspondence to:

L. Lin and B. Chen,
llin@sdust.edu.cn;
bingzhang.chen@strath.ac.uk

Citation:

Lin, L., Dong, C., Henson, S., & Chen, B. (2026). Deep learning identifies the climate warming signal in global ocean chlorophyll from satellite records. *Geophysical Research Letters*, *53*, e2025GL120669. https://doi.org/10.1029/2025GL120669

Received 20 NOV 2025
Accepted 12 FEB 2026

Author Contributions:

Conceptualization: Lei Lin
Data curation: Chen Dong
Formal analysis: Lei Lin
Funding acquisition: Lei Lin
Methodology: Lei Lin, Bingzhang Chen
Software: Chen Dong
Visualization: Chen Dong
Writing – original draft: Lei Lin, Stephanie Henson, Bingzhang Chen
Writing – review & editing: Lei Lin, Stephanie Henson, Bingzhang Chen

Abstract Satellite remote sensing of chlorophyll-a (Chl-a) provides the only continuous global-scale monitoring of phytoplankton abundance for over two decades. While certain trends have been observed in the satellite Chl-a data, it remains uncertain whether the changes are attributable to climate warming, because the data is not long enough to separate the role of climate warming from natural variability. Here, using a deep-learning model trained with an ensemble of 10 Earth System Model (ESM) simulations, we identified the climate-warming signal in satellite-derived global Chl-a fields. By comparison, a null model trained on ESM simulations forced only by natural variability was unable to identify a warming signal, confirming the role of climate warming. The warming signal is primarily derived from the spatial pattern of global Chl-a trends, and eastern and western boundary regions are most sensitive to warming. Our results explicitly reveal the ongoing climate-warming effect on global marine phytoplankton this century.

Plain Language Summary Anthropogenic climate warming is expected to influence marine phytoplankton abundance, but observational evidence has been limited by sparse data. Satellite-derived sea surface chlorophyll-a (Chl-a) offers the only continuous global-scale monitoring of phytoplankton, yet short record lengths and strong natural variability obscure long-term trends. Thus, it is challenging to detect the influence of climate warming on Chl-a from the satellite records. To address this, we developed a deep-learning model based on advanced pattern-recognition AI (artificial intelligence). Trained on a large data set from climate models' output, the AI successfully identified a climate-warming signal within the satellite Chl-a record and confirmed the effects of climate warming on the observed Chl-a change. The detected signal is primarily derived from spatial patterns of Chl-a trends, with key detection regions in eastern boundary upwelling systems and western boundary currents, implying the potential sensitivity of these regions to climate warming. This study provides novel evidence for emerging anthropogenic trends in global phytoplankton abundance.

1. Introduction

Anthropogenic greenhouse gas emissions have triggered an era of climate warming, that is, expected to change marine phytoplankton abundance and productivity by affecting water temperature, stratification, mixing, circulation, nutrient redistribution, and phytoplankton metabolism (Doney et al., 2012; Sun et al., 2024; Toseland et al., 2013; Winder & Sommer, 2012). Marine phytoplankton contribute approximately half of global primary productivity (Falkowski, 2012; Field et al., 1998), and changes to their abundance will influence the whole marine ecosystem and fishery yields (Moore et al., 2018; Tittensor et al., 2021). Therefore, it is a high priority to observe and identify the influence of climate warming on global phytoplankton.

However, it is challenging to detect the influence of climate warming from phytoplankton records due to limited temporal and spatial observational coverage. The duration of in situ observations of Chlorophyll-a concentration (Chl-a, a proxy for phytoplankton abundance) is commonly too short to unequivocally detect climate warming signals under the strong interference of natural climate variability (Cloern et al., 2024), because the warming signal is much weaker than natural variability (Sippel et al., 2020). For example, at the Bermuda Atlantic Time Series Study station, Chl-a and net primary production show an overall increasing trend from 1989 to 2007 (Saba et al., 2010), but with a rapid decrease in Chl-a after 2003 (D'Alelio et al., 2020), indicating that natural variability, rather than climate change, mainly drove the observed trends. Previous work attempted to extend Chl-a data to a century scale by combining sparse and scattered in situ Chl-a and water transparency observations or Forel-Ule scale records (e.g., Boyce et al., 2010; Wernand et al., 2013), but this approach introduced significant

uncertainty due to differing data types and temporal sampling biases (Mackas, 2011; Rykaczewski & Dunne, 2011). Moreover, long-term in situ Chl-a observations taken at fixed time series stations represent only ∼10% of the global ocean because of their limited number and restricted spatial representativeness (Henson et al., 2016).

Satellite remote sensing has provided the only continuous global observation of sea surface Chl-a over the past 20+ years, greatly enhancing our understanding of phytoplankton dynamics worldwide. However, due to the limited duration of the time series and interference from natural climate variability, climate warming signals have not been explicitly identified in satellite-derived global Chl-a data, despite the occurrence of rapid global warming and environmental changes (Cael et al., 2023; Dutkiewicz et al., 2019; Henson et al., 2010, 2017). Although some trends in Chl-a have been detected in the satellite data (e.g., Hammond et al., 2017; Zhao et al., 2025), these cannot be definitively attributed to climate warming because natural climate variability can also induce apparent Chl-a trends within the limited data span, obscuring the role of climate warming (Elsworth et al., 2020; Lin et al., 2025). Even for the mean Chl-a in basin-scale biomes, which reduces the impact of natural variability, trend analysis suggests that more than 40 yrs of satellite data may be needed to reliably distinguish the influence of climate warming from natural variability (Beaulieu et al., 2013; Henson et al., 2010; Schlunegger et al., 2020). Therefore, it remains uncertain whether global Chl-a changes observed from the limited-length satellite records are attributable to long-term climate warming.

Besides influencing the trend of phytoplankton abundance, climate warming may also affect the spatial pattern of global phytoplankton. For example, ESMs project that phytoplankton abundance will decrease in low latitudes and increase in high latitudes due to climate warming (Cabré et al., 2015; Sarmiento et al., 2004), with asymmetric changes between the Northern and Southern Hemispheres (Moore et al., 2018; Sarmiento et al., 2004) and larger shifts expected in upwelling regions (Du et al., 2024). Unlike traditional approaches that focus on the temporal variation in Chl-a time series, this study aims to detect climate warming signals from changes in the global spatial pattern of satellite-derived Chl-a using a novel deep learning method. Convolutional neural networks (CNN), one type of deep learning technique, can effectively capture spatial features in large data sets and identify weak signals amid noise, making them ideal for analyzing two-dimensional images or spatial data (Krizhevsky et al., 2017). This approach overcomes limitations of traditional trend analyses, which are constrained by low signal-to-noise ratios and short time series length, and enables the detection of climate warming signals from satellite observations of global Chl-a. Deep learning has been used to identify climate warming signals in global extreme weather events (Ham et al., 2023; Trok et al., 2024), demonstrating its potential in geoscience.

Inspired by these pioneering studies, we trained a CNN model with a large ensemble of ESM simulations forced by anthropogenic greenhouse gas emissions. This allowed the model to learn the relationships between climate warming and complex spatial patterns of global Chl-a. To tease out the effect of natural climate variability, we further trained a null CNN model using ESM simulations driven solely by natural variability without climate warming. When both CNN models were applied to satellite Chl-a data, differences between their outputs helped us identify the climate warming signal in global phytoplankton Chl-a and confirm the role of climate warming.

2. Method

2.1. Identifying the Warming Signal Using Deep Learning

We used deep learning combined with ESM simulations from the Coupled Model Intercomparison Project Phase 6 (CMIP6) to identify the climate warming signal from satellite Chl-a in three steps (Figure 1):

1. A deep learning model with a CNN algorithm was established and trained using the sea surface Chl-a concentration field and global mean near-surface temperature (GMST, a key metric for climate warming) data from simulations of the historical warming and future warming scenarios [that is, the Historical, Shared Socioeconomic Pathways 5–8.5 (SSP585), and Shared Socioeconomic Pathways 3–7.0 (SSP370) scenarios] by 10 ESMs (*see* more details in Text S1.1 and Table S1 in Supporting Information S1). Global Chl-a data was the model input, while GMST was the model output, serving as the target variable of the CNN model. This step produced a deep-learning detection model (referred to as **DD-model-1**), which encapsulates the relationship between the 2D global Chl-a patterns and GMST.
2. Two data sets of satellite-observed Chl-a (i.e., OC-CCI and MODIS, *see* more details in Text S1.2 in Supporting Information S1) were respectively projected onto this established relationship to detect signals of

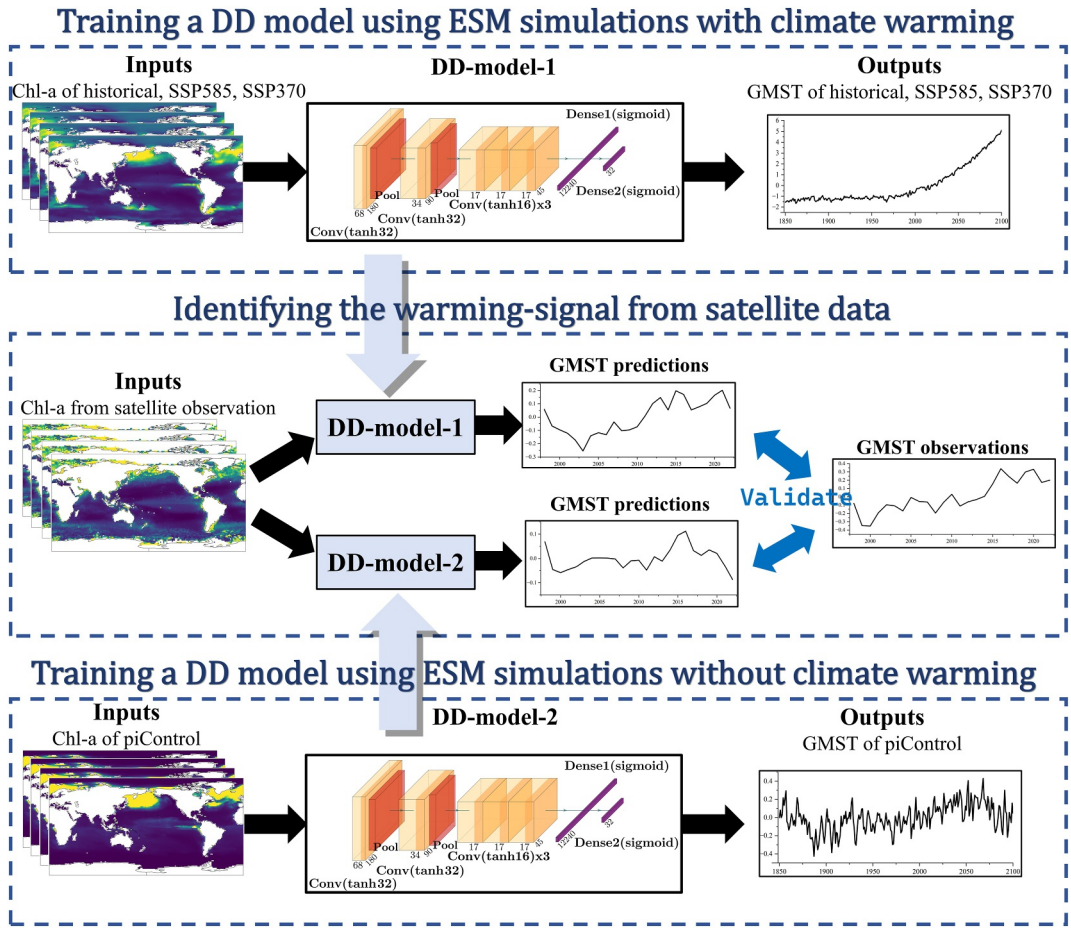

Figure 1. Schematic for using deep learning to identify climate warming signals in satellite Chl-a data. The black boxes of DD-model-1 and DD-model-2 show the structure of convolutional neural networks for the deep learning model.

climate warming. Specifically, global Chl-a fields from satellite were input into the trained DD-model-1 to predict a GMST timeseries. The predicted GMSTs were then compared with the observed GMST (Text S1.3 in Supporting Information S1) during the satellite period, particularly focusing on the warming trend in the predicted GMSTs. A significant upward trend in the GMST that exceeds the range of natural variability would indicate that the DD model successfully identifies the climate warming signal in satellite Chl-a observations.

3. A null experiment was conducted to further confirm that the detected global-warming signal by DD-model-1 reflects the effect of climate warming on phytoplankton rather than the effect of natural climate variability. In this step, a new DD model (referred to as **DD-model-2**) based on the same CNN algorithm was established and trained using the sea surface Chl-a concentration field and GMST from ESM simulations of the piControl scenario in which natural climate variability was included but climate warming forced by anthropogenic greenhouse gas emissions was excluded (Text S1.1 in Supporting Information S1). Then, the satellite Chl-a, same as (2), was fed into the DD-model-2 to predict a new GMST timeseries. If the GMST predicted by DD-model-2 has no upward trends, it would confirm that the warming signal detected by DD-model-1 from satellite Chl-a is related to climate warming, rather than being attributable to natural climate variability. Conversely, if the GMST predicted by DD-model-2 also increases with time, it suggests that the warming signal detected by DD-model-1 from satellite Chl-a cannot be attributed to long-term climate warming alone.

2.2. Construction and Training of the CNN Deep-Learning Model

We applied a CNN structure similar to Ham et al. (2023), which comprised an input layer, five convolutional layers, two pooling layers, two fully connected layers, and an output layer (Figure S1 in Supporting Information S1). The model takes standardized global sea surface Chl-a anomalies as input. Spatial features were first

extracted by two convolutional layers with 32 kernels (3×3) and a tanh activation function. Each convolutional layer is followed by a 2×2 max pooling layer with a stride of 2. Then, three convolutional layers with 16 kernels (3×3) further process the feature. The resulting feature maps are then flattened and passed through two fully connected layers with 12,240 and 32 neurons, respectively, both using sigmoid activation functions and 50% dropout for regularization. Finally, the output layer generates a scalar value representing the GMST anomaly via linear mapping. Sensitivity analysis using different layers and kernels suggests the model accuracy is not sensitive to the CNN structure (Table S2 in Supporting Information S1).

In the DD-model-1, we trained the model using the pre-processed monthly data from the Historical (1850–2014), SSP585 (2015–2100), and SSP370 (2015–2100) scenario simulations of the 10 ESMs (337-year monthly data for each model), which includes a total of 40,440 samples. The detailed procedure of the data pre-processing is introduced in Text S14 in Supporting Information S1. Training the deep learning model using simulations of these three warming scenarios can enhance its understanding of the relationship between Chl-a and GMST under varying intensities of warming forcing. Meanwhile, utilizing outputs from multiple ESMs can enable the model to account for both inter-model variability and internal climate variability, thereby enhancing its generalization capability (Madakumbura et al., 2021). DD-model-1 demonstrates a good predictive capability for GMST, with an average correlation coefficient (r) of 0.99 and an average root mean square error (RMSE) of 0.22°C across the five models in the testing (Figure S2 in Supporting Information S1). For DD-model-2, we trained the model using the piControl experiments of the same ESMs, except for missing the UKESM1-0-LL model due to a problem in downloading the metadata database. To keep consistency with DD-model-1, only 337 yrs of data in the piControl experiments for each model were used. In the testing of DD-model-2 predictions, the average r was 0.67, slightly lower than that of DD-model-1, while the average RMSE was 0.11°C, lower than that of DD-model-1 (Figure S2 in Supporting Information S1).

2.3. Occlusion Sensitivity Experiment

An occlusion sensitivity experiment is employed to quantify the relative contribution of each grid point in generating predictions from the DD-model-1, allowing for the identification of hotspots associated with the detection of the climate warming signal. The occlusion sensitivity tensor $OS(x, y)$ with regard to longitude (x) and latitude (y) is calculated by the following equation:

$$OS(x,y) = T[P(x,y)] - T[(P(x,y) * Z(7,7))] \quad (1)$$

where, $T[P(x,y)]$ is the linear trend of GMST predicted by DD-model-1 using the original Chl-a field $P(x,y)$ as input, and $T[P(x,y) * Z(7,7)]$ is the linear trend of GMST predicted by DD-model-1 using the Chl-a field covered with a 7×7 grid point occlusion as input (Ham et al., 2023). $Z(7,7)$ is the 7×7 grid point occlusion template padded with zeros, and * indicates a spatial convolution operation. The positive and negative OS values represent an underestimation and overestimation of warming trends after covering the corresponding region, respectively. The absolute value of OS can represent the regional importance for detecting the signal. In this study, we primarily focus on the absolute value of OS to identify hotspots for detecting the climate warming signal.

3. Results

3.1. Detection of Climate Warming Signals Using Deep Learning

After training with the ESM simulations, the DD-model-1 was used to identify the warming signal from two satellite Chl-a data sets (i.e., OC-CCI and MODIS). Using these data sets as input, DD-model-1 predicted two GMST results that captured the global warming trend during the satellite era (Figures 2a and 2b). Both predicted GMSTs showed a significant upward trend ($p < 0.01$), with linear increase rates of 0.013°C/yr and 0.015°C/yr for the OC-CCI and MODIS data, respectively. Although these rates were lower than the observed rate of 0.021°C/yr, the detected upward trends significantly exceed the range of internal variability of the trends in estimated GMST (Figure 3) (*see* Text S2 in Supporting Information S1 for introducing the estimation of the natural variability range), demonstrating that deep learning successfully detected climate warming signals in satellite Chl-a data. In contrast, DD-model-2, trained on the ESM simulations without the climate warming forcing, did not predict the trend in GMSTs (Figure 2c), suggesting that the effect of climate warming on global Chl-a is mainly responsible for the detected warming signal. Meanwhile, the disparity of the two models' results (i.e., Figures 2a and 2c)

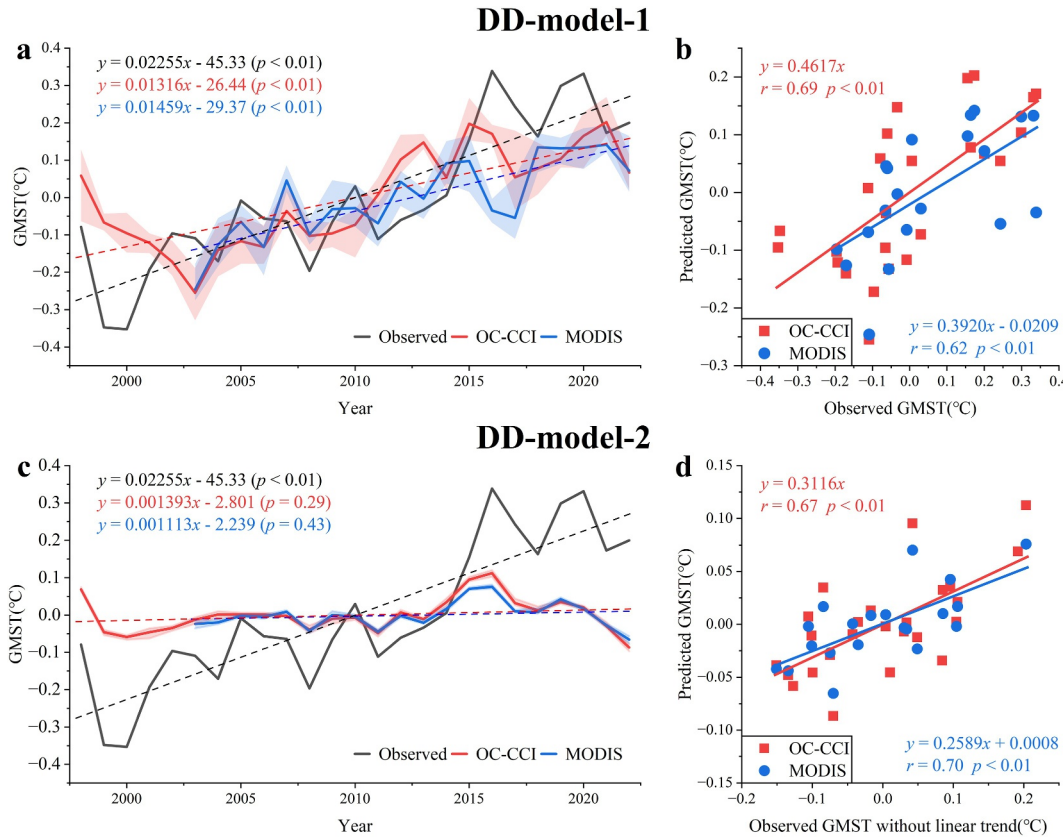

Figure 2. Deep learning identified the climate warming signals (indicated by the global mean near-surface temperature (GMST) upward trend) from satellite records of global Chl-a. (a, b) Predicted GMSTs by DD-model-1 for the OC-CCI and MODIS satellite Chl-a data and their comparisons with the observed GMST. (c, d) as (a, b), except for the predicted GMSTs by DD-model-2. DD-model-1 and DD-model-2 were trained using ESM simulations with and without climate warming processes, respectively. Note that the observed GMST in panel (d) is detrended by abstracting the linear trend from the original GMST data. The red and blue solid lines in panel (a, c) indicate the average of GMST predictions from five deep-learning models trained with different random seeds. The shaded areas denote the range of GMST predictions from these five deep-learning models. The dashed lines in panels (a, c) are the linear trends of GMSTs. The solid lines in panels (b, d) are the linear regressions of the observations and predictions.

highlights a fundamental distinction in the response of global Chl-a to climate warming compared to its response to natural climate variability.

The Pearson correlation coefficients between the predicted GMSTs and the observed GMST were 0.70 ($p < 0.01$) and 0.65 ($p < 0.01$) for the OC-CCI and MODIS data sets, respectively, indicating good predictive capability of the deep-learning model for the GMST variability (Figure 2b). Since the piControl experiment only includes natural climate variability, DD-model-2 can still capture the interannual fluctuations of GMST, as evidenced by the significant correlation between its predicted GMSTs and the detrended observed GMST (Figure 2d). In contrast, ridge regression models established using the same ESM data can not effectively predict the interannual variability of GMSTs from satellite Chl-a (Figure S4 in Supporting Information S1), indicating that simple regression detection methods are insufficient for identifying the warming signal in global Chl-a.

3.2. Timescales Attributed to the Climate Warming Signal

Chl-a variability comprises various timescales, including the long-term trend, the interannual and seasonal variations. To identify the source of the detected climate warming signal, the deep learning model was repeatedly applied to the satellite Chl-a data with different timescales. Using a Butterworth filter (B. Wang, 2024), the Chl-a timeseries was decomposed into a linear trend, interannual variation (≥12 months), and seasonal variation

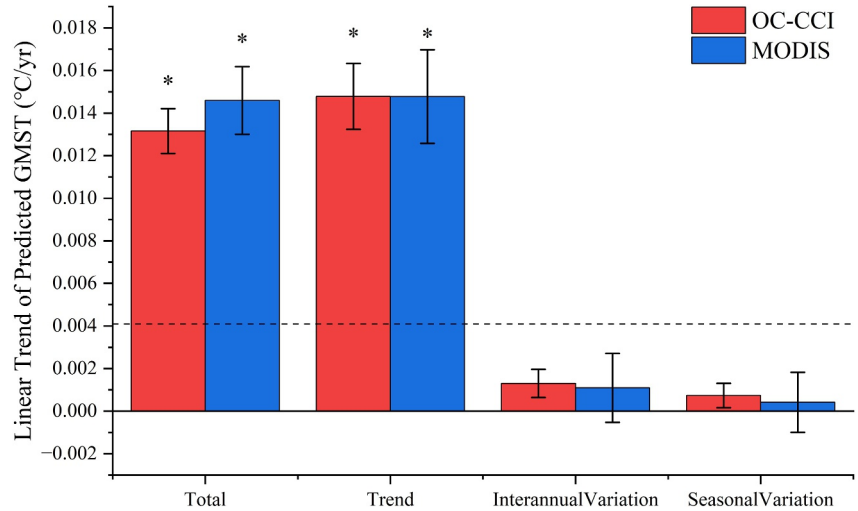

Figure 3. Global mean near-surface temperature (GMST) trends detected by DD-model-1 from the three timescale components of satellite Chl-a. Total retains all timescale components. Asterisks (*) indicate a significant upward trend in predicted GMST ($p < 0.05$). Errorbar denotes the range of GMST trends from these five deep-learning models with different random seeds. The dashed line denotes the upper bound of 95% of the natural variability of the estimated GMST linear trends by deep learning (Text S2 in Supporting Information S1).

(<12 months). Each of the temporal components was subsequently input into the DD-model-1 to predict a GMST trend.

The predicted GMST trends for the three timescale components showed that the warming signals identified by DD-model-1 primarily originated from the linear trend of the Chl-a (Figure 3 and Figure S5 in Supporting Information S1). Both the linear trend component of the OC-CCI and MODIS satellite Chl-a produced GMST trends similar to those derived from the original Chl-a data that included all timescales (Figure 3). In contrast, no significant warming signals were found in the interannual and seasonal variation components (Figure 3, Figures S5b and S5c in Supporting Information S1). These results suggest that, compared to the interannual and seasonal variations in phytoplankton, the mean state of phytoplankton could be more sensitive to global warming. Additionally, this absence of signals may also be attributed to the monthly resolution of the data used, which is insufficient for accurately capturing changes in seasonality (Henson et al., 2013).

In addition, the predicted GMSTs for the Chl-a linear trend component by DD-model-1 showed a deceleration after 2015 (Figure S5a in Supporting Information S1), which may reflect the influence of natural variability, because the DD-model-1 included the role of both climate warming and natural variability. Meanwhile, this deceleration corresponded to the decline in GMST predicted by DD-model-2 (Figure 2c), suggesting that the role of climate warming on the Chl-a trend may be partially counteracted by natural variability during this period. Nonetheless, the overall predicted GMST trend for the Chl-a linear trend was significantly greater than the natural variability range (Figure 3), highlighting the impact of climate warming on the Chl-a trend.

3.3. Hotspots for Detecting the Climate Warming Signal

We further conducted an occlusion sensitivity (OS) experiment to quantify the contributions of each spatial unit in the input field to the GMST trend predicted by DD-model-1 and to examine the hotspots associated with the detection of the climate warming signal. The OS for the two satellite Chl-a data shows a similar pattern, revealing significant spatial heterogeneity (Figures 4a and 4b). Hotspots associated with the climate warming signal are predominantly located near the eastern and western boundaries of oceans, and relatively concentrated in the northern Atlantic and Pacific. These areas, characterized by relatively high |OS| values, are crucial for detecting the warming signal. This is supported by the experiments that even when regions with low |OS| are excluded in DD-model-1, the climate warming signal remains detectable (Figure 4c). For example, when detecting the trends exclusively in areas with |OS| exceeding 0.0001 (~50% of grid cells, which is selected as an illustrative example), a significant warming trend of approximately 0.013°C per year is still evident. Sensitivity experiments conducted

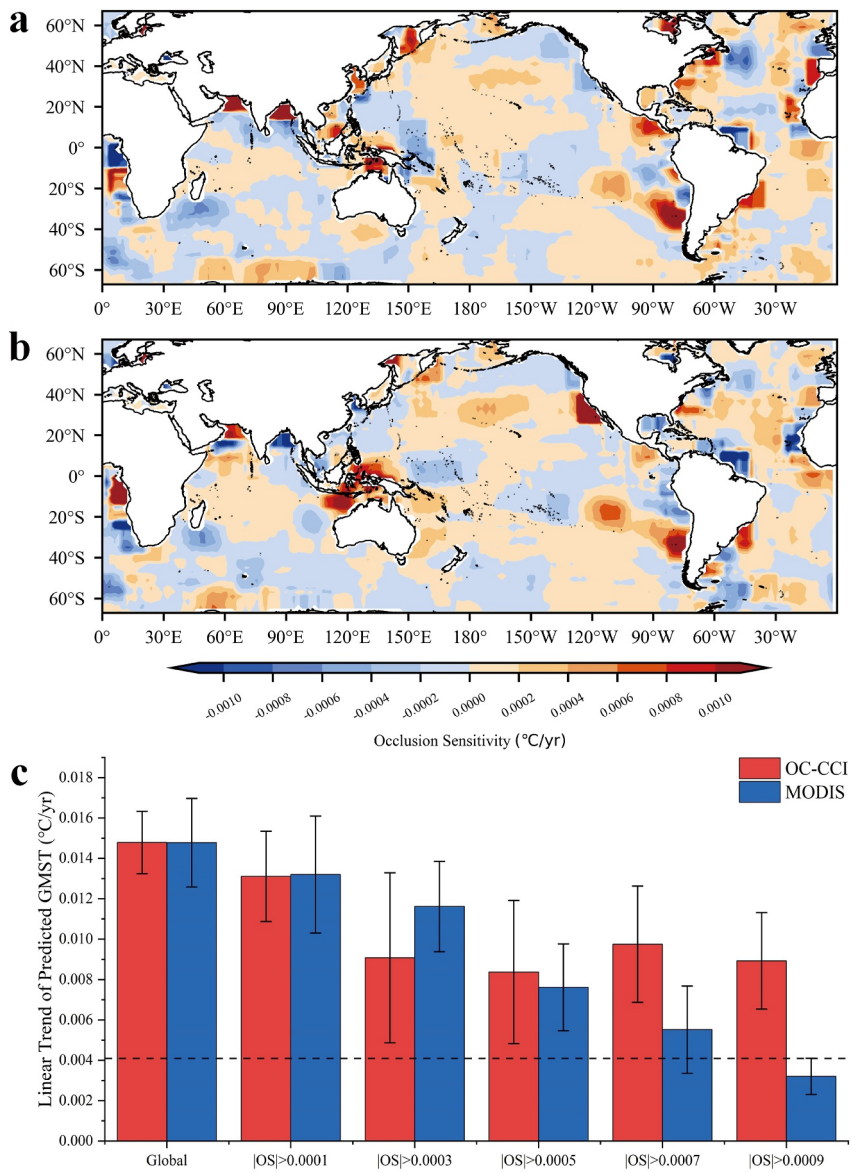

Figure 4. Occlusion sensitivity (OS in Equation 1) for the linear trend component of (a) OC-CCI and (b) MODIS Chl-a data. The value of the occlusion sensitivity denotes the changes in the predicted global mean near-surface temperature (GMST) trend after masking a 7×7 grid of points surrounding the satellite data point compared to the predicted GMST trend using the Chl-a data without masking. (c) The predicted GMST trend based solely on regions exhibiting high occlusion sensitivity. Different bars represent the results corresponding to various thresholds applied. For instance, "|OS| > 0.0001" indicates that only regions with occlusion sensitivity absolute values greater than 0.0001, as shown in panels (a, b), were included in the signal detection. "Global" indicates the case using global Chl-a data without occlusion. |OS| > 0.0001, 0.0003, 0.0005, 0.0007, and 0.0009 account for ~50%, ~16%, ~8%, ~5%, and 3% of grid cells, respectively. The dashed line in panel (c) denotes the upper bound of 95% of the natural variability of the estimated GMST linear trends by deep learning.

by incrementally increasing the |OS| threshold show that as the region detected decreases, the detected warming signal also diminishes, suggesting the importance of the spatial pattern for the warming-signal detection.

4. Discussion

In this study, the deep learning model (i.e., DD-model-1) successfully detected the climate warming signal (i.e., the predicted upward GMST) from the limited-length satellite Chl-a records. Meanwhile, the inability of DD-model-2 to detect this signal further confirms that the warming signal detected by DD-model-1 is attributed to the

role of climate warming on global Chl-a. These results demonstrate that certain changes in global Chl-a over the past two decades, though obscured by natural climate variability in short-term observations, are attributable to climate warming—indicating that its effects on phytoplankton have already emerged.

The successful detection of the warming signal stems from two key factors. First, unlike conventional time-series trend analysis, we detected the warming signal from the global Chl-a field and incorporated the spatial pattern information in the detection. The effects of climate warming and natural variability on phytoplankton could differ substantially in space, due to the distinct spatial scale of global warming versus basin-scale natural variability. For instance, in the tropical Pacific, the regression patterns of Chl-a against global warming and natural climate indices are markedly different (Lin et al., 2025). These spatial distinctions enhance the detectability of the warming signal. In contrast, traditional time-series trend analysis and simple attribution methods are limited in recognizing spatial patterns, resulting in an inability to detect the warming signal.

Second, we utilized the capacity of the CNN to learn complex relationships within large-scale climate data. Convolutional neural networks can automatically extract and categorize patterns across spatiotemporal scales through nonparametric mapping, compressing extensive global data into higher-level abstractions (Ham et al., 2023). By training the CNN on multi-scenario simulations from 10 ESMs, the model learned diverse mechanisms and acquired the ability to differentiate between the spatial signatures of climate warming and natural variability on Chl-a. As a result, the model effectively extracts robust warming fingerprints hidden in satellite observations.

The relatively coarse resolution of ESMs (typically hundreds of kilometers) limits their representation of fine-scale processes important for phytoplankton dynamics (Couespel et al., 2021; Liu et al., 2025; Wang et al., 2021). Combined with uncertainties in biogeochemical parameterizations, this can introduce biases into simulated outputs (Kwiatkowski et al., 2017; Laufkötter et al., 2015). These biases may partly explain why a deep learning model trained on ESM data underestimates the observed warming rate and projects a lower global Chl-a response to climate forcing (Figure 2a). Despite these limitations, ESMs demonstrate value by capturing key large-scale mechanisms. For instance, most ESMs can reproduce the observed short-term phytoplankton response to climate modes like El Niño–Southern Oscillation events (e.g., Kwiatkowski et al., 2017). Therefore, while acknowledging their uncertainties, ESM outputs remain valuable for training deep learning models.

The ability of the deep-learning model to detect warming signals also depends on the quality of satellite data. We applied the DD-model-1 to two additional multi-satellite merged Chl-a data sets: Data_Yu (Yu et al., 2022) and GlobColor (European Union-Copernicus Marine Service, 2022). A rising GMST of 0.011°C/yr ($p < 0.01$) was detected in the Data_Yu data set, close to the values for the OC-CCI and MODIS data sets (Figure S6 in Supporting Information S1). In contrast, no warming signal appeared in the GlobColor data set (Figure S6 in Supporting Information S1), likely attributable to data discontinuities and errors arising during the multi-satellite merging process. OC-CCI and Data_Yu applied bias-correction during the merging process to mitigate discontinuities inherent in multi-satellite data sets (Hammond et al., 2018; Yu et al., 2023), and their long-term Chl-a trends agreed with the trends from single-satellite MODIS data (Lavender et al., 2015; Lin et al., 2025; Yu et al., 2023). However, GlobColor relied on bio-optical model inversion without explicit bias-correction (Maritorena et al., 2010), leading to significant discontinuities. These discontinuities can cause a trend bias and even produce an opposite trend with other data sets (Pauthenet et al., 2024; Yu et al., 2023), especially in the tropical and subtropical North Pacific and Atlantic Oceans (Figure S7 in Supporting Information S1). Such bias may hinder the detection of climate warming signals in the GlobColor data set.

Our analysis also showed that the signals of climate warming identified in our study mainly come from the long-term trends instead of interannual or seasonal variations (Figure 3). The linear trend in satellite-derived Chl-a displays a latitude-dependent pattern, generally with decreases at low latitudes and increases at high latitudes (Zhao et al., 2025) (Figure S7 in Supporting Information S1). Overall, these asymmetric latitude trends are consistent with the responses of phytoplankton to climate warming predicted by ESMs (e.g., Cabré et al., 2015; Venegas et al., 2025). In low-latitude areas, warming increases stratification, reducing nutrient supply to the upper water column and leading to a decline in phytoplankton biomass under nutrient-limiting conditions. Conversely, in high-latitude areas, warming causes a shallower mixed layer depth and enhanced light availability in the upper water column, which boosts phytoplankton biomass under light-limited conditions (Behrenfeld et al., 2006; Doney, 2006; Winder & Sommer, 2012). Therefore, the spatial pattern of satellite-observed Chl-a trends could be

partially attributed to climate warming, implying the emergence of climate warming's impact on marine phytoplankton trends as predicted by models. However, the observed patterns of Chl-a trends also included the influence of natural variability, as evidenced by the deceleration of the predicted warming signal (Figure S5a in Supporting Information S1). To accurately characterize the true patterns of Chl-a trends driven by climate warming, extended satellite observations are necessary.

The occlusion sensitivity analysis showed that hotspots for detecting the climate warming signal are mainly located near continental margins, especially in the eastern boundary upwelling regions and western boundary current regions (Figure 4). They represent the key regions to distinguish the warming signal from natural variability. First, these regions exhibit high Chl-a concentrations and substantial interannual variability (Figure S8 in Supporting Information S1), representing an intense response to natural variability and climate warming. This enhances their utility for deep learning-based detection. Second, these regions may also be more susceptible to the impacts of climate warming. In eastern boundary upwelling regions, climate warming can significantly influence the upwelling intensity by changing wind patterns, rapidly influencing phytoplankton dynamics (Du et al., 2024). Western boundary current regions are warming at two to three times the global average ocean rate (Wu et al., 2012), which might affect the intensity and pathway of the western boundary currents, thereby impacting nutrient levels and phytoplankton biomass (e.g., Sanchez-Franks & Zhang, 2015). As a result, these ocean boundary regions deserve focused attention in the context of climate warming. Additionally, Figure 4 reveals a complex spatial pattern in the contribution of the satellite-derived Chl-a trends to the warming signal detection, with some adjacent regions even exhibiting opposing contributions. On one hand, this pattern could be associated with the interference of natural variability in these regions on the signal detection. Natural variability could lead to regionally distinct impacts on the trends in Chl-a, with some areas aligning with the long-term trend and others opposite, and thus show regionally different contributions to the warming signal detection. On the other hand, this pattern could reflect the strong regional differences and complex processes behind the influence of climate warming on phytoplankton. However, the lack of interpretability of deep learning models constrains further mechanistic insight. A more complete understanding will require longer-term observations and high-resolution mechanistic modeling.

The conclusions of this study are based on current understanding of the primary climate factors influencing phytoplankton growth and the specific hypothesis regarding climate warming's impact. Other climate change factors, such as increased CO_2 concentrations and ocean acidification, may also affect the relationship between Chl-a and GMST, though their influence is considerably weaker compared to climate warming (Beardall et al., 2009; Doney et al., 2012). Future research is needed to totally disentangle the effect of warming from those of other climate change factors.

Conflict of Interest

The authors declare no conflicts of interest relevant to this study.

Data Availability Statement

The data used in this study are freely accessible and can be downloaded from the following related websites: CMIP6 Chl-a and GMT data for the 10 ESMs (Table S1 in Supporting Information S1) were downloaded from the Earth System Grid Federation (https://esgf.github.io/nodes.html); The Chl-a data for OC-CCI, MODIS, Data_Yu, and GlobColor Chl-a data were derived from the ESA climate office (https://climate.esa.int/en/projects/ocean-color), NASA (https://oceandata.sci.gsfc.nasa.gov/), Zenodo (Yu et al., 2022), and Copernicus Marine Service (European Union-Copernicus Marine Service, 2022), respectively; and the GMST observation were downloaded from NASA (https://science.nasa.gov/earth/explore/earth-indicators/global-temperature/). The code for the deep learning model is available from Zenodo (Lin & Dong, 2026).

Acknowledgments
The authors thank the two anonymous reviewers for their insightful and constructive comments, which helped improve this paper. The authors also thank the Earth System Grid Federation, European Space Agency, National Aeronautics and Space Administration, and Copernicus Marine Service for providing access to the data. This study was supported by the National Natural Science Foundation of China (42030402) and the Open Research Fund of State Key Laboratory of Estuarine and Coastal Research (SKLEC-KF202404).

References

Beardall, J., Stojkovic, S., & Larsen, S. (2009). Living in a high CO2 world: Impacts of global climate change on marine phytoplankton. *Plant Ecology & Diversity*, *2*(2), 191–205. https://doi.org/10.1080/17550870903271363

Beaulieu, C., Henson, S. A., Sarmiento, J. L., Dunne, J. P., Doney, S. C., Rykaczewski, R. R., & Bopp, L. (2013). Factors challenging our ability to detect long-term trends in ocean chlorophyll. *Biogeosciences*, *10*(4), 2711–2724. https://doi.org/10.5194/bg-10-2711-2013

Behrenfeld, M. J., Worthington, K., Sherrell, R. M., Chavez, F. P., Strutton, P., McPhaden, M., & Shea, D. M. (2006). Controls on tropical Pacific Ocean productivity revealed through nutrient stress diagnostics. *Nature*, *442*(7106), 1025–1028. https://doi.org/10.1038/nature05083

Boyce, D. G., Lewis, M. R., & Worm, B. (2010). Global phytoplankton decline over the past century. *Nature*, *466*(7306), 591–596. https://doi.org/10.1038/nature09268

Cabré, A., Marinov, I., & Leung, S. (2015). Consistent global responses of marine ecosystems to future climate change across the IPCC AR5 earth system models. *Climate Dynamics*, *45*(5–6), 1253–1280.

Cael, B. B., Bisson, K., Boss, E., Dutkiewicz, S., & Henson, S. (2023). Global climate-change trends detected in indicators of ocean ecology. *Nature*, *619*(7970), 551–554. https://doi.org/10.1038/s41586-023-06321-z

Cloern, J. E., Schraga, T. S., Nejad, E., & Eddy, T. (2024). Phytoplankton as indicators of global warming? *Limnology and Oceanography Letters*, *9*(3), 199–208. https://doi.org/10.1002/lol2.10354

Couespel, D., Levy, M., & Bopp, L. (2021). Oceanic primary production decline halved in eddy-resolving simulations of global warming. *Biogeosciences*, *18*(14), 4321–4349. https://doi.org/10.5194/bg-18-4321-2021

D'Alelio, D., Rampone, S., Cusano, L. M., Morfino, V., Russo, L., Sanseverino, N., & Lomas, M. W. (2020). Machine learning identifies a strong association between warming and reduced primary productivity in an oligotrophic ocean gyre. *Scientific Reports*, *10*(1), 3287.

Doney, S. C. (2006). Plankton in a warmer world. *Nature*, *444*(7120), 695–696. https://doi.org/10.1038/444695a

Doney, S. C., Ruckelshaus, M., Duffy, J. E., Barry, J. P., Chan, F., English, C. A., et al. (2012). Climate change impacts on marine ecosystems. *Annual Review of Marine Science*, *4*(2012), 11–37. https://doi.org/10.1146/annurev-marine-041911-111611

Du, T., Wang, S., Jing, Z., Wu, L., Zhang, C., & Zhang, B. (2024). Future changes in coastal upwelling and biological production in eastern boundary upwelling systems. *Nature Communications*, *15*(1), 6238. https://doi.org/10.1038/s41467-024-50570-z

Dutkiewicz, S., Hickman, A. E., Jahn, O., Henson, S., Beaulieu, C., & Monier, E. (2019). Ocean colour signature of climate change. *Nature Communications*, *10*(1), 578. https://doi.org/10.1038/s41467-019-08457-x

Elsworth, G. W., Lovenduski, N. S., McKinnon, K. A., Krumhardt, K. M., & Brady, R. X. (2020). Finding the fingerprint of anthropogenic climate change in Marine Phytoplankton abundance. *Current Climate Change Reports*, *6*(2), 37–46. https://doi.org/10.1007/s40641-020-00156-w

European Union-Copernicus Marine Service. (2022). Global Ocean Colour (Copernicus-GlobColour), Bio-Geo-Chemical, L4 (monthly and interpolated) from Satellite Observations (1997-ongoing) [Dataset]. *Mercator Ocean International*. https://doi.org/10.48670/MOI-00281

Falkowski, P. (2012). Ocean Science: The power of plankton. *Nature*, *483*(7387), S17–S20. https://doi.org/10.1038/483s17a

Field, C. B., Behrenfeld, M. J., Randerson, J. T., & Falkowski, P. (1998). Primary production of the biosphere: Integrating terrestrial and Oceanic components. *Science*, *281*(5374), 237–240. https://doi.org/10.1126/science.281.5374.237

Ham, Y. G., Kim, J. H., Min, S. K., Kim, D., Li, T., Timmermann, A., & Stuecker, M. F. (2023). Anthropogenic fingerprints in daily precipitation revealed by deep learning. *Nature*, *622*(7982), 301–307. https://doi.org/10.1038/s41586-023-06474-x

Hammond, M. L., Beaulieu, C., Henson, S. A., & Sahu, S. K. (2018). Assessing the presence of discontinuities in the Ocean color satellite record and their effects on chlorophyll trends and their uncertainties. *Geophysical Research Letters*, *45*(15), 7654–7662. https://doi.org/10.1029/2017gl076928

Hammond, M. L., Beaulieu, C., Sahu, S. K., & Henson, S. A. (2017). Assessing trends and uncertainties in satellite-era ocean chlorophyll using space-time modeling. *Global Biogeochemical Cycles*, *31*(7), 1103–1117. https://doi.org/10.1002/2016gb005600

Henson, S., Cole, H., Beaulieu, C., & Yool, A. (2013). The impact of global warming on seasonality of ocean primary production. *Biogeosciences*, *10*(6), 4357–4369. https://doi.org/10.5194/bg-10-4357-2013

Henson, S. A., Beaulieu, C., Ilyina, T., John, J. G., Long, M., Séférian, R., et al. (2017). Rapid emergence of climate change in environmental drivers of marine ecosystems. *Nature Communications*, *8*(1), 14682. https://doi.org/10.1038/ncomms14682

Henson, S. A., Beaulieu, C., & Lampitt, R. (2016). Observing climate change trends in ocean biogeochemistry: When and where. *Global Change Biology*, *22*(4), 1561–1571. https://doi.org/10.1111/gcb.13152

Henson, S. A., Sarmiento, J. L., Dunne, J. P., Bopp, L., Lima, I., Doney, S. C., et al. (2010). Detection of anthropogenic climate change in satellite records of ocean chlorophyll and productivity. *Biogeosciences*, *7*(2), 621–640. https://doi.org/10.5194/bg-7-621-2010

Krizhevsky, A., Sutskever, I., & Hinton, G. E. (2017). ImageNet classification with deep convolutional neural networks. *Communications of the ACM*, *60*(6), 84–90. https://doi.org/10.1145/3065386

Kwiatkowski, L., Bopp, L., Aumont, O., Ciais, P., Cox, P. M., Laufkötter, C., et al. (2017). Emergent constraints on projections of declining primary production in the tropical oceans. *Nature Climate Change*, *7*(5), 355–358. https://doi.org/10.1038/nclimate3265

Laufkötter, C., Vogt, M., Gruber, N., Aita-Noguchi, M., Aumont, O., Bopp, L., & Völker, C. (2015). Drivers and uncertainties of future global marine primary production in marine ecosystem models. *Biogeosciences*, *12*(23), 6955–6984.

Lavender, S., Jackson, T., & Sathyendranath, S. (2015). The Ocean Colour Climate Change Initiative: Merging ocean colour observations seamlessly. *Ocean Challenge*, *21*, 29–31.

Lin, L., & Dong, C. (2026). Code for paper "Deep learning identifies the climate warming signal in global ocean chlorophyll from satellite records" [Software]. *Zenodo*. https://doi.org/10.5281/zenodo.18158124

Lin, L., Xiang, D., & Liu, D. (2025). Global warming–driven decline in phytoplankton biomass in the tropical Pacific identified from satellite records. *Journal of Geophysical Research: Biogeosciences*, *130*(7), e2025JG008743. https://doi.org/10.1029/2025jg008743

Liu, Y., He, Q., Zhan, W., Guo, M., Zheng, Y., Shen, X., & Zhan, H. (2025). Heterogeneity of phytoplankton response to submesoscale processes in the global ocean. *Communications Earth & Environment*, *6*(1), 386. https://doi.org/10.1038/s43247-025-02365-3

Mackas, D. L. (2011). Does blending of chlorophyll data bias temporal trend? *Nature*, *472*(7342), E4–E5. https://doi.org/10.1038/nature09951

Madakumbura, G. D., Thackeray, C. W., Norris, J., Goldenson, N., & Hall, A. (2021). Anthropogenic influence on extreme precipitation over global land areas seen in multiple observational datasets. *Nature Communications*, *12*(1), 3944. https://doi.org/10.1038/s41467-021-24262-x

Maritorena, S., d'Andon, O. H. F., Mangin, A., & Siegel, D. A. (2010). Merged satellite ocean color data products using a bio-optical model: Characteristics, benefits and issues. *Remote Sensing of Environment*, *114*(8), 1791–1804. https://doi.org/10.1016/j.rse.2010.04.002

Moore, J. K., Fu, W., Primeau, F., Britten, G. L., Lindsay, K., Long, M., et al. (2018). Sustained climate warming drives declining marine biological productivity. *Science*, *359*(6380), 1139–1143. https://doi.org/10.1126/science.aao6379

Pauthenet, E., Martinez, E., Gorgues, T., Roussillon, J., Drumetz, L., Fablet, R., & Roux, M. (2024). Contrasted trends in Chlorophyll-a satellite products. *Geophysical Research Letters*, *51*(14), e2024GL108916. https://doi.org/10.1029/2024gl108916

Rykaczewski, R. R., & Dunne, J. P. (2011). A measured look at ocean chlorophyll trends. *Nature*, *472*(7342), E5–E6. https://doi.org/10.1038/nature09952

Saba, V. S., Friedrichs, M. A., Carr, M. E., Antoine, D., Armstrong, R. A., Asanuma, I., et al. (2010). Challenges of modeling depth-integrated marine primary productivity over multiple decades: A case study at BATS and HOT. *Global Biogeochemical Cycles*, *24*(3). https://doi.org/10.1029/2009gb003655

Sanchez-Franks, A., & Zhang, R. (2015). Impact of the Atlantic meridional overturning circulation on the decadal variability of the Gulf Stream path and regional chlorophyll and nutrient concentrations. *Geophysical Research Letters*, *42*(22), 9889–9887. https://doi.org/10.1002/2015gl066262

Sarmiento, J. L., Slater, R., Barber, R., Bopp, L., Doney, S. C., Hirst, A. C., et al. (2004). Response of ocean ecosystems to climate warming. *Global Biogeochemical Cycles*, *18*(3), 2003GB002134. https://doi.org/10.1029/2003gb002134

Schlunegger, S., Rodgers, K. B., Sarmiento, J. L., Ilyina, T., Dunne, J. P., Takano, Y., et al. (2020). Time of emergence and large ensemble intercomparison for Ocean biogeochemical trends. *Global Biogeochemical Cycles*, *34*(8), e2019GB006453. https://doi.org/10.1029/2019gb006453

Sippel, S., Meinshausen, N., Fischer, E. M., Székely, E., & Knutti, R. (2020). Climate change now detectable from any single day of weather at global scale. *Nature Climate Change*, *10*(1), 35–41. https://doi.org/10.1038/s41558-019-0666-7

Sun, S., Thompson, A. F., Yu, J., & Wu, L. (2024). Transient overturning changes cause an upper-ocean nutrient decline in a warming climate. *Nature Communications*, *15*(1), 7727. https://doi.org/10.1038/s41467-024-52200-0

Tittensor, D. P., Novaglio, C., Harrison, C. S., Heneghan, R. F., Barrier, N., Bianchi, D., et al. (2021). Next-generation ensemble projections reveal higher climate risks for marine ecosystems. *Nature Climate Change*, *11*(11), 973–981. https://doi.org/10.1038/s41558-021-01173-9

Toseland, A. D. S. J., Daines, S. J., Clark, J. R., Kirkham, A., Strauss, J., Uhlig, C., et al. (2013). The impact of temperature on marine phytoplankton resource allocation and metabolism. *Nature Climate Change*, *3*(11), 979–984. https://doi.org/10.1038/nclimate1989

Trok, J. T., Barnes, E. A., Davenport, F. V., & Diffenbaugh, N. S. (2024). Machine learning–based extreme event attribution. *Science Advances*, *10*(34), eadl3242. https://doi.org/10.1126/sciadv.adl3242

Venegas, R. M., Rivas, D., & Treml, E. (2025). Global climate-driven sea surface temperature and chlorophyll dynamics. *Marine Environmental Research*, *204*, 106856. https://doi.org/10.1016/j.marenvres.2024.106856

Wang, B. (2024). Signal processing based on butterworth filter: Properties, design, and applications. Highlights in science. *Engineering and Technology*, *97*, 72–77. https://doi.org/10.54097/3cq7qb95

Wang, J., Liu, Z., Foster, I., Chang, W., Kettimuthu, R., & Kotamarthi, V. (2021). Fast and accurate learned multiresolution dynamical downscaling for precipitation. *Geoscientific Model Development*, *14*(10), 6355–6372. https://doi.org/10.5194/gmd-14-6355-2021

Wernand, M. R., van der Woerd, H. J., & Gieskes, W. W. (2013). Trends in ocean colour and chlorophyll concentration from 1889 to 2000, worldwide. *PLoS One*, *8*(6), e63766. https://doi.org/10.1371/journal.pone.0063766

Winder, M., & Sommer, U. (2012). Phytoplankton response to a changing climate. *Hydrobiologia*, *698*(1), 5–16.

Wu, L., Cai, W., Zhang, L., Nakamura, H., Timmermann, A., Joyce, T., et al. (2012). Enhanced warming over the global subtropical western boundary currents. *Nature Climate Change*, *2*(3), 161–166. https://doi.org/10.1038/nclimate1353

Yu, S., Bai, Y., He, X., Gong, F., & Li, T. (2023). A new merged dataset of global ocean chlorophyll-a concentration for better trend detection. *Frontiers in Marine Science*, *10*, 1051619. https://doi.org/10.3389/fmars.2023.1051619

Yu, S., et al. (2022). A new merged dataset of global ocean chlorophyll-a concentration for better trend detection (monthly V1.0) [Dataset]. *Zenodo*. https://doi.org/10.5281/zenodo.7092220

Zhao, H., Manizza, M., Lozier, M. S., & Cassar, N. (2025). Greener green and bluer blue: Ocean poleward greening over the past two decades. *Science*, *388*(6753), 1337–1340. https://doi.org/10.1126/science.adr9715

References From the Supporting Information

Hansen, J., Ruedy, R., Sato, M., & Lo, K. (2010). *Current GISS global surface temperature analysis*. NASA Goddard Institute for Space Studies.